Fault Current and Voltage Estimation Method in Symmetrical Monopolar MMC-based DC Grids

Jingqiu Yu, *Member*, *IEEE*, Zheren Zhang, *Member*, *IEEE*, and Zheng Xu, *Fellow*, *IEEE*

***Abstract*—Symmetrical monopolar configuration is the prevailing scheme configuration for modular multilevel converter based high-voltage direct current (MMC-HVDC) links, in which severe DC overvoltage or overcurrent can be caused by the DC faults. To deal with the possible asymmetry in the DC faults and the coupling effects of the DC lines, this paper analyzes the DC fault characteristics based on the phase-mode transformation. First, the DC grid is decomposed into the common-mode and the differential-mode networks. The equivalent models of the MMCs and DC lines in the two networks are derived, respectively. Then, based on the state matrices, a unified numerical calculation method for the fault voltages and currents at the DC side is proposed. Compared with the time-domain simulations performed on PSCAD/EMTDC, the accuracy of the proposed method is validated. Last, the system parameter analysis shows that the grounding parameters play an important role in reducing the severity of the pole-to-ground faults, whereas the coupling effects of the DC lines should be considered when calculating the DC fault currents associated with the pole-to-pole faults.**

***Index Terms*—Symmetrical monopolar DC grids, modular multilevel converter (MMC), pole-to-ground fault, pole-to-pole faults, phase-mode transformation, fault current and voltage estimation.**

I. Introduction

VOLTAGE source converter based high-voltage direct current (VSC-HVDC) grids are a powerful candidate for the integration of massive amounts of renewable energy and the interconnection of asynchronous AC grids [1], [2]. Due to the high reliability and flexibility, the modular multilevel converter (MMC) has drawn more and more attention from both academia and industry [3]. Among the commissioned MMC-HVDC links, symmetrical monopolar configuration is the most widely-used scheme [4]-[6]. However, the MMC-based DC grid, which is a development trend of the VSC-HVDC, is facing challenges caused by the DC faults [7].

Typical DC faults include pole-to-ground (PTG) faults and pole-to-pole (PTP) faults [8]. PTG faults make the symmetrical monopolar DC grids suffer from pole imbalances and therefore severe overvoltage on the healthy pole. PTP faults are more likely to result in severe overcurrent. For the proper design of system parameters and protection configuration, it is vital to evaluate the overvoltage and the overcurrent levels caused by the DC faults with some calculation methods. A majority of researches have paid attention to the calculation of PTP faults as they pose stringent requirements on the breaking current of DC circuit breakers (DCCBs) [9]-[11]. Some studies on PTG faults in symmetrical monopolar DC grids have also been performed. The mechanism of the overvoltage caused by DC faults is explained in [12], while system studies related to insulation coordination aspects of DC cable systems and converter equipment are conducted in [13]-[16] and [17], respectively. The overvoltage at the cable terminations is studied for selected fault types by simulations in these studies. To calculate the maximum overvoltage, MMC is modeled considering the relative size between the impedance of MMC and the grounding device in the fault network in [18].

Generally speaking, the research on the calculation of transient characteristics with PTG faults in symmetrical monopolar DC grids has not been deeply studied, considering the following difficulties: ① the asymmetrical property of PTG faults and the coupling effects of DC lines make the fault characteristics of the positive and negative poles unbalanced and coupled; ② the variety of topologies increases the difficulty in forming a unified method for arbitrary HVDC grids. Up to now, for the proper design of system parameters and selective protection employing DCCBs, an analytical calculation method dealing with the pole imbalances and coupling issues for symmetrical monopolar DC grids has not been studied. In this paper, this problem is solved and the further attempt is also performed to analyze the fault characteristics for both PTG and PTP faults in symmetrical monopolar DC grids. The main contributions are as follows.

1) The common-mode and differential-mode equivalent models of the MMC-based DC grid are derived from the original circuits based on the phase-mode transformation. The phase-mode transformation is widely used in the AC transmission systems with the coupled multiple lines to derive their decoupled models. In this paper, the phase-mode transformation is adopted to deal with the asymmetrical property of PTG faults and the coupling effects of DC lines, and the original MMC-based DC grid can be decomposed into decoupled common-mode and differential-mode networks.

Manuscript received: January 31, 2021; revised: April 11, 2021; accepted: June 29, 2021. Date of CrossCheck: June 29, 2021. Date of online publication: September 7, 2021.

J. Yu, Z. Zhang, and Z. Xu (corresponding author) are with the Department of Electrical Engineering, Zhejiang University, Hangzhou, China (e-mail: yujingqiu@zju.edu.cn; zhangzheren@zju.edu.cn; xuzheng007@zju.edu.cn).

DOI: 10.35833/MPCE.2021.000077

2) The general way based on the state matrices is proposed to study the fault characteristics suitable for arbitrary HVDC topologies. By listing the basic differential equations of the networks, the analysis on the variation of the fault characteristics with different system parameters can be easily conducted. This is helpful for the proper design of system parameters such as the grounding parameters and the coupling parameters.

The remainder of this paper is organized as follows. Section II derives the equivalent model of MMCs and DC lines in the common-mode and differential-mode networks. The fault behavior is investigated simultaneously. Section III establishes the connection of the common-mode and differential-mode networks according to different fault boundary conditions. Section IV gives the unified method for computing the DC fault currents and voltages by listing the state matrices. In Section V, time-domain simulations of PTG faults and PTP faults in a four-terminal DC grid are carried out based on PSCAD/EMTDC to verify the accuracy of the proposed method. The research on the influence on the fault characteristics by the variation of the grounding parameters and the DC line mutual inductance are conducted then. Section VI draws the conclusions.

II. HVDC Grid Modeling Based on Phase-mode Transformation

A. Basic Principle of Phase-mode Transformation

In the symmetrical monopolar HVDC system, PTG faults are treated as asymmetrical faults, whereas PTP faults belong to symmetrical faults. The phase-mode transformation proposed in [19], [20] is able to cover the fault transient analysis for both the symmetrical and asymmetrical faults.

The basic principle for phase-mode transformation is that an arbitrary pair of the positive-pole and negative-pole variables can be decomposed into one couple of the common-mode and differential-mode variables, as shown in Fig. 1, where the symbols "p" and "n" denote the positive pole and negative-pole variables, respectively; and the subscripts "com" and "dif" denote the common-mode and differential-mode variables, respectively.

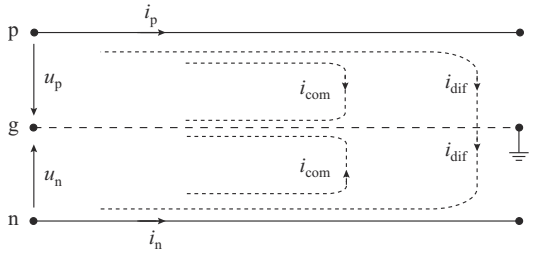

Fig. 1. Phase-mode transformation of branch currents.

Taking the positive-pole and negative-pole currents as an example, the transformation can be expressed as:

$$\begin{bmatrix} i_{com} \\ i_{dif} \end{bmatrix} = \frac{1}{2}\begin{bmatrix} 1 & 1 \\ 1 & -1 \end{bmatrix}\begin{bmatrix} i_p \\ i_n \end{bmatrix} \tag{1}$$

It can be found in Fig. 1 that the common-mode currents are just the unbalanced components between the positive-pole and negative-pole currents that flow through the earth, which are actually the zero-sequence components. The differential-mode currents are the balanced components flowing only through the DC lines, which are actually the positive-sequence components. In other words, the phase-mode transformation resolves the positive-pole and negative-pole values into the zero-sequence and positive-sequence components, respectively. Thus, the symmetrical monopolar HVDC system can be represented in terms of their zero-sequence and positive-sequence networks connected in different ways depending on the types of the DC faults.

B. Phase-mode Transformation of MMC Stations

At present, there are three main grounding schemes for symmetrical monopolar HVDC systems. The first one is grounding through star-connected reactors and a large resistor at the AC side. The second one is adopting a resistor at the neutral point of transformer (delta/star configuration) at the AC side. The third one is using two large resistors in parallel at the DC side [21]. The fault characteristics at the DC side of the first and the second grounding schemes are similar. A zero-sequence fault current could flow through the grounding devices causing pole imbalances in these two grounding schemes [22]. The third grounding scheme would result in additional losses and the two serial DC resistors would probably lead to the voltage imbalance due to a certain amount of resistance deviation. In high-voltage and large-capacity MMC-HVDC systems, the former two grounding schemes are widely used in many practical projects. Since the first and the second grounding schemes have similar DC fault characteristics, in this paper, the first grounding scheme is taken as an example for phase-mode transformation.

In the symmetrical monopolar MMC-HVDC system, the first grounding scheme consists of the star-connected grounding reactors L_0 with a series-connected grounding resistor R_0 at the valve side of the converter transformer, as illustrated in Fig. 2 [6]. The MMC consists of six arms, where the upper and lower arms in the same phase form a phase unit. Each arm consists of two parts, i.e., N series-connected identical sub-modules (SMs) and an arm inductor L_{arm}. The equivalent arm resistor and the SM capacitor are denoted as R_{arm} and C_0, respectively.

In Fig. 2, u_{rj} and i_{rj} ($j=$a, b, c; $r=$p, n) are the upper- and lower-arm voltages and currents, respectively; i_{vj} is the AC output current of MMC in phase j; u_{vj} is the AC voltage at the point of common coupling (PCC) in phase j; and i_0 is the current flowing through the grounding device at the valve side. According to the Kirchhoff's voltage law, the mathematical model in phase j could be derived as:

$$u_{vj} - L_{arm}\frac{di_{pj}}{dt} - R_{arm}i_{pj} + u_{pj} = u_p \tag{2}$$

$$u_{vj} - L_{arm}\frac{di_{nj}}{dt} - R_{arm}i_{nj} - u_{nj} = u_n \tag{3}$$

Based on (2) and (3), the mathematical equations (4) and (5) describing the model of MMC at the DC side can be derived, and the details are shown in Appendix A.

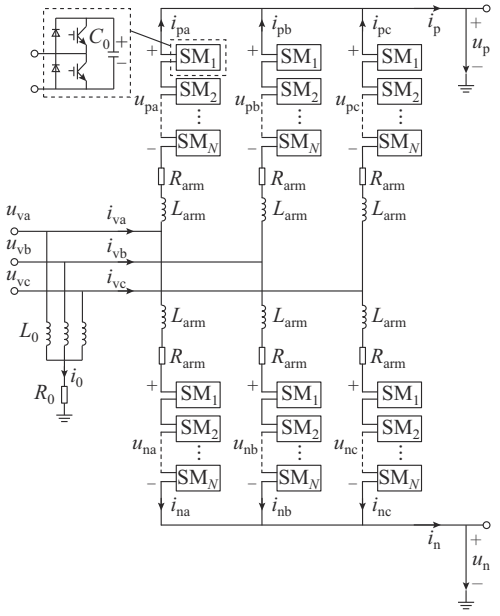

Fig. 2. Basic structure of MMC.

$$\begin{cases} u_{v0}-\dfrac{R_{arm}}{3}i_{com}-\dfrac{L_{arm}}{3}\dfrac{di_{com}}{dt}+u_{Ceqcom}=u_{com} \\ u_{Ceqcom}=\dfrac{1}{6}\displaystyle\sum_{j=a,b,c}(u_{pj}-u_{nj}) \end{cases} \tag{4}$$

$$\begin{cases} -\dfrac{R_{arm}}{3}i_{dif}-\dfrac{L_{arm}}{3}\dfrac{di_{dif}}{dt}+u_{Ceqdif}=u_{dif} \\ u_{Ceqdif}=\dfrac{1}{6}\displaystyle\sum_{j=a,b,c}(u_{pj}+u_{nj}) \end{cases} \tag{5}$$

where u_{Ceqdif} is the average value of the total arm voltages in three phases; and u_{Ceqcom} is the average value of the imbalance between the upper- and lower-arm voltages in three phases. The zero-sequence component of the valve-side voltage u_{v0} can be expressed as:

$$u_{v0}=\frac{L_0}{3}\frac{di_0}{dt}+R_0i_0=-\frac{2L_0}{3}\frac{di_{com}}{dt}-2R_0i_{com} \tag{6}$$

For the second grounding scheme, u_{v0} could be calculated by the common-mode currents and the resistor of the transformer star winding at the secondary side. To obtain the DC-side equivalent common-mode and differential-mode models, the following reasonable assumptions are conducted. Firstly, the high-order harmonic components (twice the fundamental frequency and above) in the circulating current are ignored [23]. Secondly, the high-order harmonic components of the output voltage of the upper and lower arms are omitted [24]. Finally, the fundamental modulated signal of MMC is symmetrically balanced [25]. The modulation signal m_j in phase j is defined as:

$$m_j=M\cos(\omega t+\varphi_j) \tag{7}$$

where M is the modulation ratio; ω is the fundamental angular frequency; and φ_j is the initial phase.

1) Differential-mode Network

The upper- and lower-arm voltages satisfy the following relationships [26]:

$$\begin{cases} u_{pj}=m_{pj}u_{pj}^{\Sigma}=\dfrac{1-m_j}{2}u_{pj}^{\Sigma} \\ \dfrac{du_{pj}^{\Sigma}}{dt}=-\dfrac{Nm_{pj}}{C_0}i_{pj} \end{cases} \tag{8}$$

$$\begin{cases} u_{nj}=m_{nj}u_{nj}^{\Sigma}=\dfrac{1+m_j}{2}u_{nj}^{\Sigma} \\ \dfrac{du_{nj}^{\Sigma}}{dt}=\dfrac{Nm_{nj}}{C_0}i_{nj} \end{cases} \tag{9}$$

where u_{pj}^{Σ} and u_{nj}^{Σ} are the total voltages of N SM capacitors in the upper and lower arms, respectively; and m_{pj} and m_{nj} are the SM input ratios of the upper and lower arms, respectively.

Then the expression describing the dynamic characteristic of u_{Ceqdif} can be derived as (10). For simplicity, the voltage imbalance between the upper and lower arms is ignored.

$$u_{Ceqdif}=\frac{1}{6}\sum_{j=a,b,c}\left(u_{pj}+u_{nj}\right)=\frac{1}{6}\sum_{j=a,b,c}\left(\frac{u_{pj}^{\Sigma}+u_{nj}^{\Sigma}}{2}-\frac{u_{pj}^{\Sigma}-u_{nj}^{\Sigma}}{2}m_j\right)=\frac{1}{12}\sum_{j=a,b,c}\left(u_{pj}^{\Sigma}+u_{nj}^{\Sigma}\right) \tag{10}$$

Then, taking the derivative of (10) and substituting (8) and (9) into it, (11) can be derived as:

$$\begin{aligned}\frac{du_{Ceqdif}}{dt}&=\frac{N}{12C_0}\sum_{j=a,b,c}\left(-m_{pj}i_{pj}+m_{nj}i_{nj}\right)=\\&\frac{N}{12C_0}\sum_{j=a,b,c}\left(\frac{i_{pj}+i_{nj}}{2}m_j-\frac{i_{pj}-i_{nj}}{2}\right)=\\&\frac{N}{12C_0}\left(\frac{\sum_{j=a,b,c}u_{vj}i_{vj}}{u_{Ceqdif}}-i_{dif}\right)=\frac{N}{12C_0}\left(\frac{p_s}{u_{Ceqdif}}-i_{dif}\right)\end{aligned} \tag{11}$$

where p_s is the active power transmitted from AC side to DC side. As described in (12), it can be approximately calculated under the active power control and DC voltage control [27].

$$p_s=\begin{cases} P_s^{ref} & \text{active power control} \\ 1.5u_{sd}i_{sd}^{ref} & \text{DC voltage control} \end{cases} \tag{12}$$

where P_s^{ref} is the reference power; u_{sd} is the d-axis voltage; $i_{sd}^{ref}=k_p\left(u_{dc}^{ref}-u_{dc}(t)\right)+k_i\int\left(u_{dc}^{ref}-u_{dc}(t)\right)dt$ is the d-axis reference current, and k_p and k_i are the proportional and integral coefficients of the DC voltage controller, respectively; u_{dc} is the DC voltage of MMC; and u_{dc}^{ref} is the reference DC voltage of MMC.

Then, based on (5) and (11), the differential-mode equivalent model of MMC could be derived, as shown in Fig. 3.

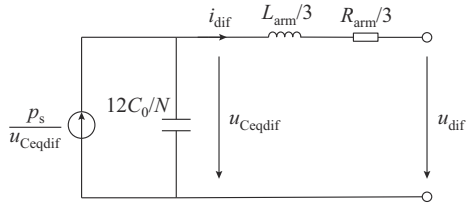

Fig. 3. Differential-mode equivalent model of MMC.

2) Common-mode Network

Based on the above assumptions, the currents through the upper and lower arms can be expressed as:

$$\begin{cases} i_{\mathrm{p}j} = \dfrac{i_{\mathrm{v}j}}{2} + \dfrac{i_{\mathrm{p}}}{3} \\ i_{\mathrm{n}j} = \dfrac{i_{\mathrm{v}j}}{2} + \dfrac{i_{\mathrm{n}}}{3} \end{cases} \tag{13}$$

Then, the currents through the SM capacitors can be derived as:

$$\begin{cases} i_{\mathrm{cp}j} = m_{\mathrm{p}j} i_{\mathrm{p}j} = \left(\dfrac{1}{2} - \dfrac{m_j}{2}\right)\left(\dfrac{i_{\mathrm{v}j}}{2} + \dfrac{i_{\mathrm{p}}}{3}\right) \\ i_{\mathrm{cn}j} = m_{\mathrm{n}j} i_{\mathrm{n}j} = \left(\dfrac{1}{2} + \dfrac{m_j}{2}\right)\left(\dfrac{i_{\mathrm{v}j}}{2} + \dfrac{i_{\mathrm{n}}}{3}\right) \end{cases} \tag{14}$$

where $i_{\mathrm{cp}j}$ is the SM capacitor current in the upper arm of phase j; and $i_{\mathrm{cn}j}$ is the SM capacitor current in the lower arm of phase j.

Therefore, the DC and fundamental frequency fluctuation of the SM capacitor voltages in the upper and lower arms can be calculated as:

$$\begin{cases} \Delta u_{\mathrm{cp}j}^{(0)} = -\dfrac{1}{6C_0}\displaystyle\int\left(i_{\mathrm{p}} - i_{\mathrm{dc}}\right)\mathrm{d}t \\ \Delta u_{\mathrm{cn}j}^{(0)} = \dfrac{1}{6C_0}\displaystyle\int\left(i_{\mathrm{n}} - i_{\mathrm{dc}}\right)\mathrm{d}t \end{cases} \tag{15}$$

$$\begin{cases} \Delta u_{\mathrm{cp}j}^{(1)} = -\dfrac{1}{\omega C_0}\displaystyle\int\left(\frac{i_{\mathrm{v}j}}{4} - \frac{i_{\mathrm{p}}}{6}\right)\mathrm{d}t \\ \Delta u_{\mathrm{cn}j}^{(1)} = \dfrac{1}{\omega C_0}\displaystyle\int\left(\frac{i_{\mathrm{v}j}}{4} + \frac{i_{\mathrm{n}}}{6}\right)\mathrm{d}t \end{cases} \tag{16}$$

where the superscripts 0 and 1 represent the DC and fundamental components, respectively; and i_{dc} is the steady-state current of the DC lines.

Then, the voltages of the upper and lower arms could be derived as:

$$\begin{cases} u_{\mathrm{p}j} = N m_{\mathrm{p}j}\left(u_{\mathrm{cN}} + \Delta u_{\mathrm{cp}j}^{(0)} + \Delta u_{\mathrm{cp}j}^{(1)}\right) \\ u_{\mathrm{n}j} = N m_{\mathrm{n}j}\left(u_{\mathrm{cN}} + \Delta u_{\mathrm{cn}j}^{(0)} + \Delta u_{\mathrm{cn}j}^{(1)}\right) \end{cases} \tag{17}$$

where u_{cN} is the rated voltage of SM capacitors.

Therefore, u_{Ceqcom} is expressed as:

$$u_{\mathrm{Ceqcom}} = \frac{1}{6}\sum_{j=\mathrm{a,b,c}}\left(u_{\mathrm{p}j} - u_{\mathrm{n}j}\right) = -\frac{N}{24C_0}\int\left(i_{\mathrm{p}} + i_{\mathrm{n}}\right)\mathrm{d}t = -\frac{N}{12C_0}\int i_{\mathrm{com}}\,\mathrm{d}t \tag{18}$$

It can be seen from (18) that the unbalanced current between the positive and negative poles drives the asymmetry of pole voltages. This zero-sequence current also causes the imbalance of the SM capacitor voltages in the upper and the lower arms. Based on (4), (6), and (18), the common-mode network of MMC could be derived, as shown in Fig. 4.

C. Phase-mode Transformation of DC Lines

The lumped π-type model shows a little bias in estimating the fault characteristics compared with the frequency dependent model. Therefore, considering the sufficient accuracy, the π-type equivalent model of a DC line used in [9], [27], [28] is employed in this paper, as shown in Fig. 5, where L_{dc} is the smoothing reactor; R_{ij}, L_{ij}, and C_{ij} are the equivalent resistance, inductance, and capacitance of the π-type model, respectively; and $C_{\mathrm{M}ij}$ and M_{ij} are the mutual capacitance and inductance of the DC lines, respectively.

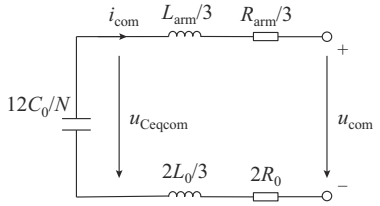

Fig. 4. Common-mode equivalent model of MMC.

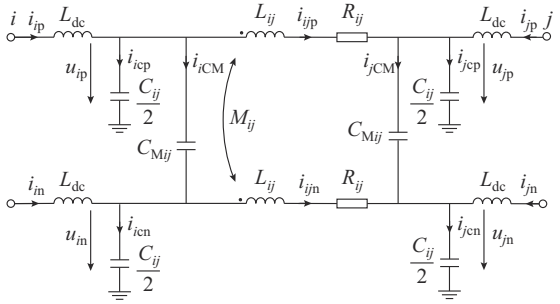

Fig. 5. Lumped π-type model of DC lines with coupling effects.

The equations governing the characteristics of DC lines can be written as:

$$\begin{bmatrix} u_{i\mathrm{p}} - u_{j\mathrm{p}} \\ u_{i\mathrm{n}} - u_{j\mathrm{n}} \end{bmatrix} = \begin{bmatrix} L_{ij} & M_{ij} \\ M_{ij} & L_{ij} \end{bmatrix}\frac{\mathrm{d}}{\mathrm{d}t}\begin{bmatrix} i_{ij\mathrm{p}} \\ i_{ij\mathrm{n}} \end{bmatrix} + R_{ij}\begin{bmatrix} i_{ij\mathrm{p}} \\ i_{ij\mathrm{n}} \end{bmatrix} \tag{19}$$

$$\frac{\mathrm{d}}{\mathrm{d}t}\begin{bmatrix} u_{i\mathrm{p}} & u_{i\mathrm{n}} & u_{j\mathrm{p}} & u_{j\mathrm{n}} \end{bmatrix}^{\mathrm{T}} = \mathrm{diag}\left(\frac{2}{C_{ij}}\right)\begin{bmatrix} i_{i\mathrm{cp}} & i_{i\mathrm{cn}} & i_{j\mathrm{cp}} & i_{j\mathrm{cn}} \end{bmatrix}^{\mathrm{T}} \tag{20}$$

$$\frac{\mathrm{d}}{\mathrm{d}t}\begin{bmatrix} u_{i\mathrm{p}} - u_{i\mathrm{n}} & u_{j\mathrm{p}} - u_{j\mathrm{n}} \end{bmatrix}^{\mathrm{T}} = \mathrm{diag}\left(\frac{1}{C_{\mathrm{M}ij}}\right)\begin{bmatrix} i_{i\mathrm{CM}} & i_{j\mathrm{CM}} \end{bmatrix}^{\mathrm{T}} \tag{21}$$

$$\begin{cases} i_{i\mathrm{p}} = i_{i\mathrm{cp}} + i_{i\mathrm{CM}} + i_{ij\mathrm{p}} \\ i_{i\mathrm{n}} = i_{i\mathrm{cn}} - i_{i\mathrm{CM}} + i_{ij\mathrm{n}} \\ i_{j\mathrm{p}} = i_{j\mathrm{cp}} + i_{j\mathrm{CM}} - i_{ij\mathrm{p}} \\ i_{j\mathrm{n}} = i_{j\mathrm{cn}} - i_{j\mathrm{CM}} - i_{ij\mathrm{n}} \end{cases} \tag{22}$$

where $u_{i\mathrm{p}}$, $u_{i\mathrm{n}}$, $u_{j\mathrm{p}}$, and $u_{j\mathrm{n}}$ are the positive-pole and negative-pole node voltages, respectively; $i_{i\mathrm{cp}}$, $i_{i\mathrm{cn}}$, $i_{j\mathrm{cp}}$, and $i_{j\mathrm{cn}}$ are the branch currents through the grounding capacitance $C_{ij}/2$; $i_{i\mathrm{CM}}$ and $i_{j\mathrm{CM}}$ are the branch currents through the phase-to-phase capacitance $C_{\mathrm{M}ij}$; $i_{ij\mathrm{p}}$ and $i_{ij\mathrm{n}}$ are the positive-pole and negative-pole currents of RL branches, respectively; and $i_{i\mathrm{p}}$, $i_{i\mathrm{n}}$, $i_{j\mathrm{p}}$, and $i_{j\mathrm{n}}$ are the positive-pole and negative-pole branch currents through nodes i and j, respectively.

It can be observed from (19)-(22) that the coupling issue makes it hard to solve the fault characteristics of the positive or negative pole independently. However, it can be dealt with by applying the phase-mode transformation.

$$\begin{bmatrix} u_{i\mathrm{com}} - u_{j\mathrm{com}} \\ u_{i\mathrm{dif}} - u_{j\mathrm{dif}} \end{bmatrix} = \begin{bmatrix} L_{ij} + M_{ij} & 0 \\ 0 & L_{ij} - M_{ij} \end{bmatrix}\frac{\mathrm{d}}{\mathrm{d}t}\begin{bmatrix} i_{ij\mathrm{com}} \\ i_{ij\mathrm{dif}} \end{bmatrix} + R_{ij}\begin{bmatrix} i_{ij\mathrm{com}} \\ i_{ij\mathrm{dif}} \end{bmatrix} \tag{23}$$

$$\frac{\mathrm{d}}{\mathrm{d}t}\begin{bmatrix} u_{i\mathrm{com}} \\ u_{i\mathrm{dif}} \\ u_{j\mathrm{com}} \\ u_{j\mathrm{dif}} \end{bmatrix} = \mathrm{diag}\left(\frac{2}{C_{ij}}, \frac{1}{\frac{C_{ij}}{2}+2C_{\mathrm{M}ij}}, \frac{2}{C_{ij}}, \frac{1}{\frac{C_{ij}}{2}+2C_{\mathrm{M}ij}} \right) \begin{bmatrix} i_{i\mathrm{com}} - i_{ij\mathrm{com}} \\ i_{i\mathrm{dif}} - i_{ij\mathrm{dif}} \\ i_{j\mathrm{com}} + i_{ij\mathrm{com}} \\ i_{j\mathrm{dif}} + i_{ij\mathrm{dif}} \end{bmatrix} \tag{24}$$

Thus, based on (23) and (24), the correspondingly decoupled equivalent models of DC lines are given in Fig. 6.

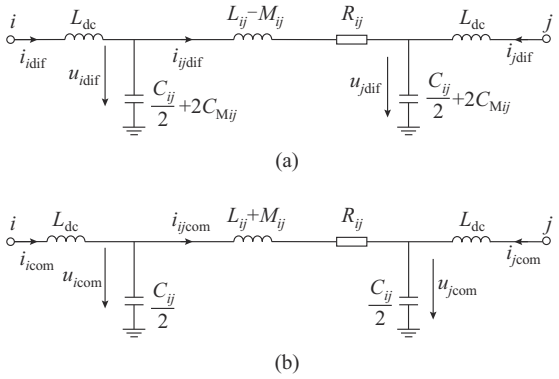

Fig. 6. Decoupled equivalent models of DC lines. (a) Differential-mode equivalent model. (b) Common-mode equivalent model.

III. Fault Boundary Conditions

Based on the phase-mode transformation, the original network can be represented with two independent networks. And they are connected through the fault boundary conditions based at the various types of faults. The following types of faults at the DC side are mainly considered in this paper, i.e., PTG faults and PTP faults.

A. PTG Faults

The simplified diagram of the PTG fault is shown in Fig. 7(a), where R_f is the grounding resistor. When a positive PTG fault occurs, the instantons boundary conditions satisfy:

$$\begin{cases} u_{f\mathrm{p}} = R_f i_{f\mathrm{p}} \\ i_{f\mathrm{n}} = 0 \end{cases} \tag{25}$$

The corresponding fault conditions for the common-mode and differential-mode components are expressed as:

$$\begin{cases} u_{f\mathrm{com}} + u_{f\mathrm{dif}} = R_f\left(i_{f\mathrm{com}} + i_{f\mathrm{dif}}\right) \\ i_{f\mathrm{com}} - i_{f\mathrm{dif}} = 0 \end{cases} \tag{26}$$

Equation (26) makes it easy to form the connection of the common-mode and differential-mode networks, as shown in Fig. 7(b). All desired voltages and currents can be calculated with the circuit in Fig. 7(b). It should be noted that when a PTG fault occurs on the negative pole, (25) should be modified as:

$$\begin{cases} u_{f\mathrm{com}} - u_{f\mathrm{dif}} = R_f\left(i_{f\mathrm{com}} - i_{f\mathrm{dif}}\right) \\ i_{f\mathrm{com}} + i_{f\mathrm{dif}} = 0 \end{cases} \tag{27}$$

Equation (27) shows that under a negative PTG fault, the common-mode and differential-mode networks should be connected in parallel via $2R_f$.

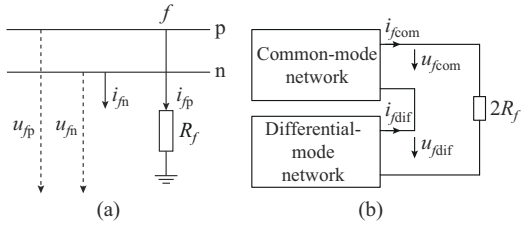

Fig. 7. Fault boundary conditions for PTG faults. (a) Circuit diagram. (b) Connection of differential-mode and common-mode networks.

B. PTP Faults

When a PTP fault occurs, the fault boundary conditions are depicted in Fig. 8(a), which can be expressed as:

$$\begin{cases} i_{f\mathrm{p}} = -i_{f\mathrm{n}} \\ u_{f\mathrm{p}} - u_{f\mathrm{n}} = i_{f\mathrm{p}} R_f \end{cases} \tag{28}$$

By making phase-mode transformation to (28), we can obtain:

$$\begin{cases} i_{f\mathrm{com}} = 0 \\ u_{f\mathrm{dif}} = \dfrac{R_f}{2} i_{f\mathrm{dif}} \end{cases} \tag{29}$$

Therefore, it is easy to provide the connection between the common-mode and differential-mode networks under PTP faults with (29), as shown in Fig. 8(b).

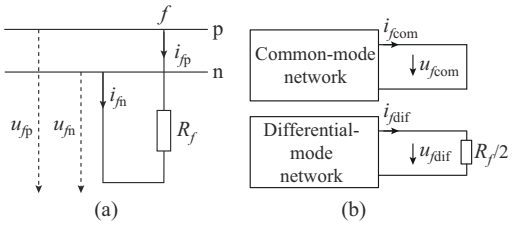

Fig. 8. Fault boundary conditions for PTP faults. (a) Circuit diagram. (b) Connection of differential-mode and common-mode networks.

IV. Fault Current and Voltage Calculation

According to the transformed model of MMCs, DC lines, and fault boundary conditions, the equivalent networks of the whole grid can be established. And from the perspective of the individual networks, the pole imbalance and coupling issues are solved, which is beneficial for computing the fault current and voltage.

In the equivalent circuit model of a symmetrical monopolar DC grid with arbitrary topologies, there are four kinds of circuits, including the equivalent model of MMC and line-to-ground capacitance (circuit ①), the π-type equivalent model of DC lines (circuit ②), the line-to-ground capacitances of line connections (circuit ③), and the fault boundary conditions (circuit ④), as shown in Fig. 9. The state matrices for fault currents and voltages are easy to be obtained. Since the differential-mode and common-mode networks are only different in the MMC parameters and DC line parameters, in this section, we only give the list of the state equations for the differential-mode network.

Here, MMC nodes and line connection nodes are named from 1 to n. The positive direction of the currents is defined as flowing out of the nodes, whereas the positive direction

of the currents through the branches are defined from node i to node j. The defined nodes and currents are expressed in Fig. 9. In Fig. 9, i, j, p, q, s, t, f, and m are the defined nodes. The current symbols with the subscript "L" mean the currents through the smoothing reactors, such as $i_{iq\mathrm{L}}$, $i_{ip\mathrm{L}}$, $i_{ij\mathrm{L}}$, $i_{ji\mathrm{L}}$, $i_{fi\mathrm{L}}$, and $i_{fs\mathrm{L}}$. The current symbols without the subscript "L" mean the branch currents through the DC lines such as i_{ij}. The voltage symbols with the subscript "M" are the voltages through the equivalent capacitor of MMC. The voltage symbols without the subscript "M" are the voltages through the equivalent capacitor of the DC lines.

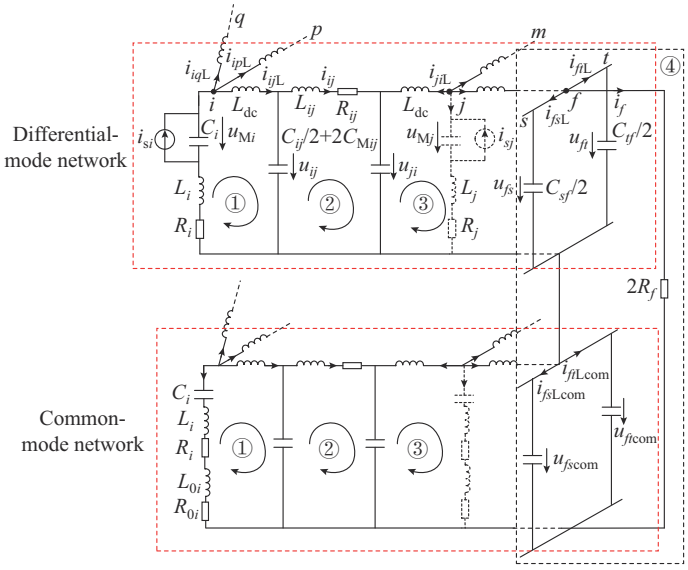

Fig. 9. Equivalent model of whole DC grid under PTG faults.

A. Circuit ①

For circuit ①, the state variables for currents are those flowing through smoothing reactors from nodes to DC lines.

$$\dot{\boldsymbol{i}}_{\mathrm{Ldc}}=\begin{bmatrix}\cdots & \dot{i}_{ij\mathrm{L}} & \dot{i}_{ip\mathrm{L}} & \dot{i}_{iq\mathrm{L}} & \cdots\end{bmatrix}^{\mathrm{T}} \tag{30}$$

The state variables for voltages are those of the capacitors.

$$\dot{\boldsymbol{u}}=\begin{bmatrix}\cdots & \dot{u}_{\mathrm{M}i} & \dot{u}_{\mathrm{M}j} & \cdots & \dot{u}_{ij} & \dot{u}_{ji} & \cdots\end{bmatrix}^{\mathrm{T}} \tag{31}$$

Therefore, the state matrix is expressed as:

$$\dot{\boldsymbol{i}}_{\mathrm{Ldc}}=\boldsymbol{L}_1[\boldsymbol{i}_{\mathrm{Ldc}}\quad \boldsymbol{i}_{\mathrm{LR}}\quad \boldsymbol{u}]^{\mathrm{T}} \tag{32}$$

$$\boldsymbol{C}\dot{\boldsymbol{u}}=\boldsymbol{A}[\boldsymbol{i}_{\mathrm{Ldc}}\quad \boldsymbol{i}_{\mathrm{LR}}\quad \boldsymbol{i}_{\mathrm{s}}]^{\mathrm{T}} \tag{33}$$

where $\boldsymbol{i}_{\mathrm{Ldc}}=\begin{bmatrix}\cdots & i_{ij\mathrm{L}} & i_{ip\mathrm{L}} & i_{iq\mathrm{L}} & \cdots\end{bmatrix}^{\mathrm{T}}$ is the branch current vector through the smoothing reactors; $\boldsymbol{i}_{\mathrm{LR}}=\begin{bmatrix}\cdots & i_{ij} & i_{ip} & i_{iq} & \cdots\end{bmatrix}^{\mathrm{T}}$ is the branch current vector through π-type sections; $\boldsymbol{u}=\begin{bmatrix}\cdots & u_{\mathrm{M}i} & u_{\mathrm{M}j} & \cdots & u_{ij} & u_{ji} & \cdots\end{bmatrix}^{\mathrm{T}}$ is the voltage vector across the capacitors; $\boldsymbol{C}=\mathrm{diag}\begin{bmatrix}\cdots & C_i & C_j & \cdots & C_{ij}/2+2C_{\mathrm{M}ij} & C_{ij}/2+2C_{\mathrm{M}ij} & \cdots\end{bmatrix}$ is the network capacitance matrix; and $\boldsymbol{i}_{\mathrm{s}}=\begin{bmatrix}\cdots & i_{si} & i_{sj} & \cdots\end{bmatrix}^{\mathrm{T}}$ is the equivalent current source vector. The elements in $\boldsymbol{A}$ and $\boldsymbol{L}_1$ are expressed in (34) and Table I, respectively. In Table I, $k\in i$ means node k is directly connected to node i; and m means the number of such nodes. Their matrix forms are shown in Appendix B.

$$A_{ij}=\begin{cases}1 & \text{current flowing into capacitor } C_{ii} \text{ of } \boldsymbol{C}\\ -1 & \text{current flowing out of capacitor } C_{ii} \text{ of } \boldsymbol{C}\\ 0 & \text{others}\end{cases} \tag{34}$$

TABLE I
ELEMENTS IN $\boldsymbol{L}_1$ CORRESPONDING TO ROW OF $\dot{\boldsymbol{i}}_{\mathrm{Ldc}}$

Variables		Element
Branch current	$i_{ik\mathrm{L}}$ $(k\in i)$	$-\dfrac{R_i}{L_{\mathrm{dc}}+mL_i}$
	$i_{pq\mathrm{L}}$ $(p\neq i)$	0
	i_{ik}	0
	i_{pq}	0
Capacitor voltage	u_{ij}	$-\dfrac{L_{\mathrm{dc}}+(m-1)L_i}{(L_{\mathrm{dc}}+mL_i)L_{\mathrm{dc}}}$
	u_{ik} $(k\in i\&k\neq j)$	$\dfrac{L_i}{(L_{\mathrm{dc}}+mL_i)L_{\mathrm{dc}}}$
	$u_{\mathrm{M}i}$	$\dfrac{1}{L_{\mathrm{dc}}+mL_i}$
	$u_{\mathrm{M}p}$	0
	u_{pq}	0

B. Circuit ②

For circuit ②, the state variables for currents are those flowing through π-type sections of DC lines.

$$\dot{\boldsymbol{i}}_{\mathrm{LR}}=\begin{bmatrix}\cdots & \dot{i}_{ij} & \dot{i}_{ip} & \dot{i}_{iq} & \cdots\end{bmatrix}^{\mathrm{T}} \tag{35}$$

Then, the state matrix can be written as:

$$\dot{\boldsymbol{i}}_{\mathrm{LR}}=\boldsymbol{L}_2[\boldsymbol{i}_{\mathrm{LR}}\quad \boldsymbol{u}]^{\mathrm{T}} \tag{36}$$

The elements in $\boldsymbol{L}_2$ are given in Table II and the matrix form is shown in Appendix B.

TABLE II
ELEMENTS IN $\boldsymbol{L}_2$ CORRESPONDING TO ROW OF $\dot{\boldsymbol{i}}_{\mathrm{LR}}$

Variables	Element
i_{ij}	$-\dfrac{R_{ij}}{L_{ij}-M_{ij}}$
u_{ij}	$\dfrac{1}{L_{ij}-M_{ij}}$
u_{ji}	$-\dfrac{1}{L_{ij}-M_{ij}}$

C. Circuit ③

For line connection nodes, there are only circuits composed of line-to-ground capacitances. However, if virtual MMCs are assumed to be connected as shown in Fig. 9 (indicated by dotted line), then the state matrix equations for circuit ③ can be listed just in the same way as circuit ①. And the equivalent parameters L_j and C_j are set as infinity, whereas R_j and i_{sj} are set as 0.

D. Circuit ④

As described in Section III, the fault boundary conditions are to connect the differential-mode and common-mode networks. This part is different from the former three circuits,

which depends on the fault type, for example, a positive PTG fault occurs on line l_{st}. This produces a new line connection node f and new voltage state variables in both two networks. However, the new variables $i_{fs\mathrm{L}}$ and $i_{ft\mathrm{L}}$ in the differential-mode network will not be state variables. Thus, there should be supplementary algebraic equations.

$$\begin{cases} \dfrac{C_{sf}}{2}\dot{u}_{fs} = i_{fs\mathrm{L}} + i_{sf} \\ \dfrac{C_{tf}}{2}\dot{u}_{ft} = i_{ft\mathrm{L}} + i_{tf} \\ u_{fs} = u_{ft} \end{cases} \tag{37}$$

$$\begin{cases} i_{fs\mathrm{L}} + i_{ft\mathrm{L}} = i_{fs\mathrm{Lcom}} + i_{ft\mathrm{Lcom}} \\ u_{fs} + u_{fs\mathrm{com}} = -2R_f(i_{fs\mathrm{L}} + i_{ft\mathrm{L}}) \end{cases} \tag{38}$$

For other types of faults, just replace (38) with the fault boundary equations. For the common-mode network, only some parameters need to be modified: $\boldsymbol{i}_{\mathrm{s}}$ is replaced with $\mathbf{0}$; L_i and R_i are substituted for $L_i + L_{0i}$ and $R_i + R_{0i}$, respectively; $L_{ij} - L_{\mathrm{M}ij}$ and $C_{ij}/2 + 2C_{\mathrm{M}ij}$ are replaced with $L_{ij} + L_{\mathrm{M}ij}$ and $C_{ij}/2$, respectively. The fault voltage and current can be computed by the sums and differences of the node voltages and branch currents in the differential-mode and common-mode variables.

V. Case Studies

A. Test System

To verify the accuracy of the proposed method in calculating the fault voltages and currents in symmetrical monopolar DC grids, the simulations of a four-terminal MMC-based DC grid are conducted by PSCAD. Figure 10 gives the structure of this grid. The main parameters are listed in Table III.

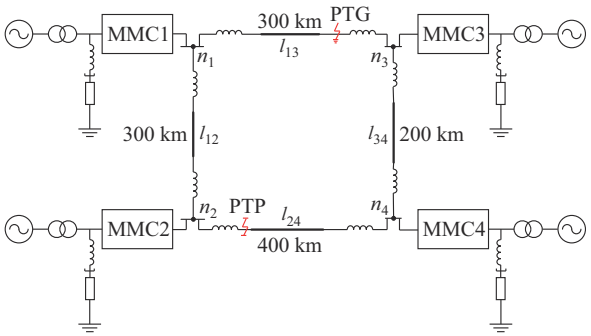

Fig. 10. Four-terminal symmetrical monopolar MMC-based DC grid.

PTG faults in symmetrical monopolar DC grids result in severe overvoltage and pole imbalances, whereas PTP faults generate very large short-circuit currents. Therefore, the DC grids should isolate the faults as quickly as possible. In fact, for DC grids using DCCBs to deal with DC faults, one of the basic principles is that the converter station should not be blocked before DCCB opening [25], [29], [30]. Generally, due to the communication system, the DCCBs receive the action signal and then execute the command with a delay. When the DC faults are isolated by the DCCBs, the voltage and current are supposed to be decreased. Therefore, this paper focuses on the fault characteristics prior to the action of DCCBs. The duration is taken as 10 ms in this paper [9].

TABLE III
Main Circuit Parameters of Test System

	Items	Values
Converter stations	Rated voltage of AC system	220 kV
	Nominal ratio of transformer	220 kV/210 kV
	Leakage inductance of transformer	15%
	Smoothing reactor	300 mH
	Rated capacity (MMC1&MMC3)	750 MVA
	Rated capacity (MMC2&MMC4)	1500 MVA
	Grounding inductance	3 H
	Grounding resistance	1000 Ω
	Rated DC voltage	±200 kV
	Arm inductor (MMC1&MMC3)	66 mH
	Arm inductor (MMC2&MMC4)	32 mH
	SM capacitor (MMC1&MMC3)	12000 μF
	SM capacitor (MMC2&MMC4)	18000 μF
	Number of SMs per arm	150
DC transmission lines	Resistance	0.014 Ω/km
	Self-inductance	0.82 mH/km
	Mutual-inductance	0.24 mH/km
	Capacitance	0.01367 μF/ km
Control mode	MMC1	$Q=0$ Mvar, $P=-600$ MW
	MMC2	$Q=0$ Mvar, $P=-1200$ MW
	MMC3	$Q=0$ Mvar, $U_{\mathrm{dc}}=\pm 200$ kV
	MMC4	$Q=0$ Mvar, $P=1500$ MW

B. Validation Results

1) PTG Faults

As shown in Fig. 10, a PTG fault at the outlet side is set on line l_{13}. According to the proposed method based on the derived models, the state equations (32), (33), and (36)-(38) are solved by MATLAB. The fault currents and voltages are calculated in two cases with low fault resistance ($R_f = 0.01$ Ω) and high fault resistance ($R_f = 100$ Ω). The calculation results and simulation results by PSCAD/EMTDC are shown in Fig. 11, where $u_{1\mathrm{n}}$ is the healthy PTG voltage of MMC1; $u_{4\mathrm{n}}$ is the healthy PTG voltage of MMC4; i_{13} is the current through line l_{13}; i_{24} is the current through line l_{24}, and simulation and calculation values are distinguished by superscripts "s" and "c", respectively.

The branch currents and voltages of the remote and nearby DC lines are depicted. In Fig. 11(a) and (c), the maximum relative error for fault voltages does not exceed 2.5%, whereas the error for fault current is less than 3%. This indicates the fault currents and voltages obtained from the calculation and simulation are in satisfactory match with negligible errors. Similar conclusions can also be drawn from the case of high fault resistance.

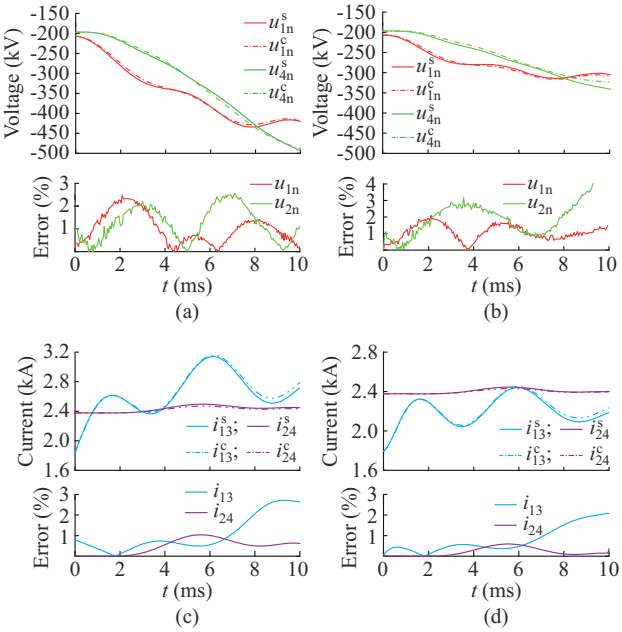

Fig. 11. Comparisons of healthy PTG voltages and branch currents in two cases. (a) Voltage results with R_f=0.01 Ω. (b) Voltage results with R_f=100 Ω. (c) Current results with R_f=0.01 Ω. (d) Current results with R_f=100 Ω.

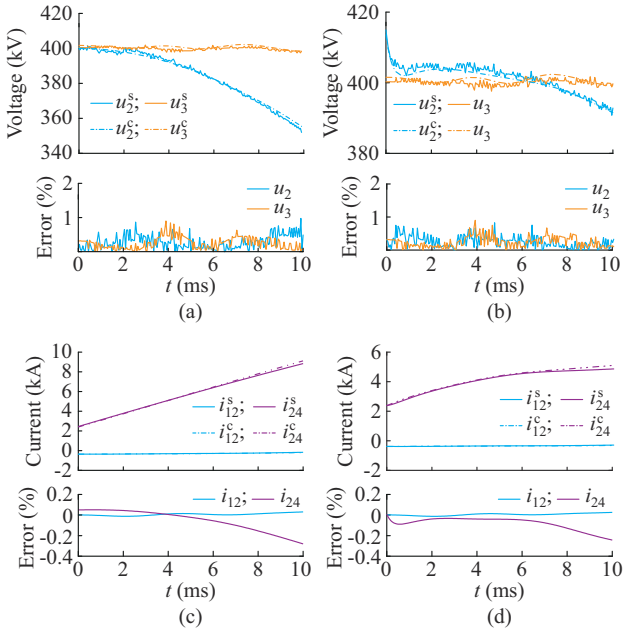

Fig. 12. Comparisons of PTP voltages and branch currents in two cases. (a) Voltage results with R_f=0.01 Ω. (b) Voltage results with R_f=100 Ω. (c) Current results with R_f=0.01 Ω. (d) Current results with R_f=100 Ω.

2) PTP Faults

As shown in Fig. 10, a PTP fault at the outlet side is set on line l_{24}. The simulation and calculation results in two cases with low fault resistance (R_f=0.01 Ω) and high fault resistance (R_f=100 Ω) are shown in Fig. 12, where u_2 is the PTP voltage of MMC2; u_3 is the PTP voltage of MMC3; i_{12} is the current through line l_{12}; and i_{24} is the current through line l_{24}. The relative errors for the PTP voltages are less than 1%, whereas the relative errors for the branch currents of the DC lines are no more than 0.3%. This proves the accuracy in estimating the fault characteristics under PTP faults.

3) Analysis of Results

The error between the simulation and calculation comes from the assumptions for ignoring the high-order harmonic components in deriving the MMC model. And the π-type model of the DC lines also leads to some bias arising from neglecting the impacts of frequency on line parameters and traveling wave phenomena. Besides, the errors for the fault currents and voltages are more obvious beyond 10 ms after the fault because the assumptions on which the model is derived are broken.

It should also be noted that the maximum overvoltage of the healthy pole under the PTG faults has not yet appeared within 10 ms, as shown in Fig. 11. The maximum fault current under the PTP faults has not appeared either, as shown in Fig. 12. This relates with the configuration and action of the protection system, such as the action time of circuit breakers. Though the maximum values have not appeared in the observation time range, the development of the fault current and voltage before the action of DCCBs could be clearly observed. Therefore, the proposed method is available for protection system design since the development process determines the maximum overvoltage and overcurrent.

Above all, it can be concluded that the proposed method based on phase-mode transformation is able to provide accurate fault currents and voltages before the protection action under the PTG and PTP faults. Besides, it is appropriate to use this method for the design of system parameters.

C. Sensitivity Analysis of System Parameters

For PTG faults, the zero-sequence currents result in the imbalances between the SM capacitor voltages of different poles, which are the currents through the grounding devices at the AC side. Besides, the healthy pole suffers from serious overvoltage. But reasonable configuration of system parameters may improve this situation. For PTP faults, the fault current can be several times the normal current. It is of special interest for DCCB design to know the dynamic profiles of in the stage of fault current system design.

1) Influence of Grounding Parameters

Due to the fact that the zero-sequence currents only occur under asymmetrical faults, for PTP faults, there are no such pole imbalance issues. Here, the severity of the PTG fault in DC grid with varying grounding device parameters can be observed in Fig. 13.

The maximum grounding current and the maximum overvoltage are contradictory to each other. Besides, the grounding reactor has weaker effect in reducing the grounding current and overvoltage compared with the grounding resistance. They can be chosen to guarantee that the overvoltage and grounding current are within their specified ranges. The selected system parameters are able to release the burden of protection system. Besides, the parameters can also be optimized if other factors such as cost and steady-state power loss are taken into account with some optimal algorithms.

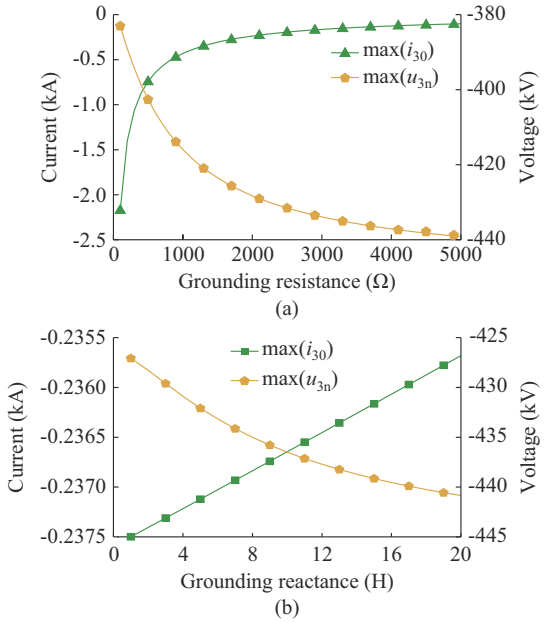

Fig. 13. The maximum healthy PTG voltage u_{3n} and the maximum grounding current i_{30} of MMC3. (a) Varying grounding resistance. (b) Varying grounding inductance.

2) *Influence of Mutual Inductance of DC Lines*

The influence of the mutual inductance variation for PTP faults is shown in Fig. 14. As illustrated in Fig. 14, the mutual inductance is bad for limiting the fault current. This is because there is a strong demagnetization effect due to the opposite direction of the currents through lines of the positive and negative poles. Besides, there is a positive linear correlation between the maximum current and the mutual inductance. Therefore, the mutual inductance is vital for determining the capacity of DCCB under PTP faults.

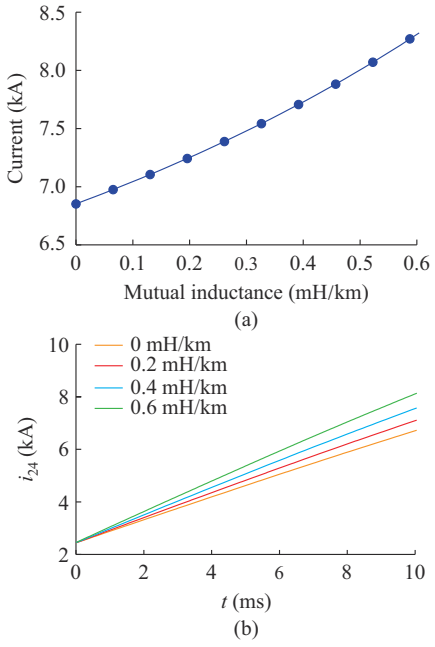

Fig. 14. Influence of mutual inductance for PTP faults. (a) The maximum branch current max(i_{24}). (b) Branch current i_{24} with different mutual inductances.

As depicted in Fig. 15(a), compared with the grounding device, the mutual inductance plays little role in reducing the pole imbalances or the overvoltage for PTG faults. It should also be noted in Fig. 15(b) that the time for the peak fault current varies with the mutual inductance, but the amplitude nearly remains the same. Therefore, it can be concluded that mutual inductance variation of DC lines could be neglected in the design of grounding parameters or the protection system parameters for PTG faults.

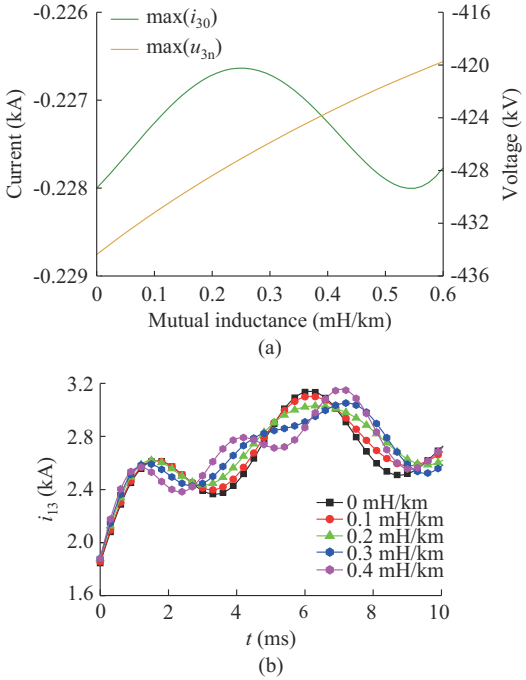

Fig. 15. Influence of mutual inductance under PTG faults. (a) The maximum grounding current i_{30} and healthy PTG voltage u_{3n} of MMC3. (b) Branch current i_{13} with different mutual inductances.

VI. Conclusion

This paper offers a way to analytically study the PTG and PTP fault characteristics for symmetric monopolar MMC-based HVDC grids. Following conclusions can be drawn through both theoretical analysis and simulation studies.

1) Based on the phase-mode transformation, the coupling issues and pole imbalances are eliminated in the derived common-mode and differential-mode networks. Compared with PSCAD/EMTDC simulations, for cases of high and low fault resistance, the errors for the fault voltages and currents under PTG faults are less than 3%, whereas the errors under PTP faults are less than 1%, which shows sufficient accuracy.

2) Parameter variation analysis can be easily conducted relying on the calculation method based on state equations. It is shown that under PTG faults, the grounding resistance is more significant than the grounding reactor in reducing the pole imbalances and overvoltage. Under PTP faults, the maximum fault current increases linearly with the mutual inductance.

APPENDIX A

For each phase, there is an equation in the same form as (2) and (3). By adding the three-phase equations of (2) and (3), we can obtain:

$$\sum_{j=\mathrm{a,b,c}} u_{\mathrm{v}j} - L_{\mathrm{arm}} \frac{\mathrm{d}\sum\limits_{j=\mathrm{a,b,c}} i_{\mathrm{p}j}}{\mathrm{d}t} - R_{\mathrm{arm}} \sum_{j=\mathrm{a,b,c}} i_{\mathrm{p}j} + \sum_{j=\mathrm{a,b,c}} u_{\mathrm{p}j} = 3u_{\mathrm{p}} \tag{A1}$$

$$\sum_{j=\mathrm{a,b,c}} u_{\mathrm{v}j} - L_{\mathrm{arm}} \frac{\mathrm{d}\sum\limits_{j=\mathrm{a,b,c}} i_{\mathrm{n}j}}{\mathrm{d}t} - R_{\mathrm{arm}} \sum_{j=\mathrm{a,b,c}} i_{\mathrm{n}j} - \sum_{j=\mathrm{a,b,c}} u_{\mathrm{n}j} = 3u_{\mathrm{n}} \tag{A2}$$

According to the Kirchhoff's current law, the arm currents satisfy the following relationship:

$$\begin{cases} \sum\limits_{j=\mathrm{a,b,c}} i_{\mathrm{p}j} = i_{\mathrm{p}} \\ \sum\limits_{j=\mathrm{a,b,c}} i_{\mathrm{n}j} = i_{\mathrm{n}} \end{cases} \tag{A3}$$

For unbalanced AC systems, the sum of the three-phase voltage is three times that of a single zero-sequence voltage.

$$\sum_{j=\mathrm{a,b,c}} u_{\mathrm{v}j} = 3u_{\mathrm{v0}} \tag{A4}$$

Substituting (A3) and (A4) into (A1) and (A2), we can obtain:

$$u_{\mathrm{v0}} - \frac{L_{\mathrm{arm}}}{3}\frac{\mathrm{d}i_{\mathrm{p}}}{\mathrm{d}t} - \frac{R_{\mathrm{arm}}}{3} i_{\mathrm{p}} + \frac{1}{3}\sum_{j=\mathrm{a,b,c}} u_{\mathrm{p}j} = u_{\mathrm{p}} \tag{A5}$$

$$u_{\mathrm{v0}} - \frac{L_{\mathrm{arm}}}{3}\frac{\mathrm{d}i_{\mathrm{n}}}{\mathrm{d}t} - \frac{R_{\mathrm{arm}}}{3} i_{\mathrm{n}} - \frac{1}{3}\sum_{j=\mathrm{a,b,c}} u_{\mathrm{n}j} = u_{\mathrm{n}} \tag{A6}$$

Adding (A5) and (A6), we have:

$$u_{\mathrm{v0}} - \frac{L_{\mathrm{arm}}}{6}\frac{\mathrm{d}\left(i_{\mathrm{p}} + i_{\mathrm{n}}\right)}{\mathrm{d}t} - \frac{R_{\mathrm{arm}}}{6}\left(i_{\mathrm{p}} + i_{\mathrm{n}}\right) + \frac{1}{6}\sum_{j=\mathrm{a,b,c}}\left(u_{\mathrm{p}j} - u_{\mathrm{n}j}\right) = \frac{u_{\mathrm{p}} + u_{\mathrm{n}}}{2} \tag{A7}$$

Subtracting (A6) from (A5), we have:

$$-\frac{L_{\mathrm{arm}}}{6}\frac{\mathrm{d}\left(i_{\mathrm{p}} - i_{\mathrm{n}}\right)}{\mathrm{d}t} - \frac{R_{\mathrm{arm}}}{6}\left(i_{\mathrm{p}} - i_{\mathrm{n}}\right) + \frac{1}{6}\sum_{j=\mathrm{a,b,c}}\left(u_{\mathrm{p}j} + u_{\mathrm{n}j}\right) = \frac{u_{\mathrm{p}} - u_{\mathrm{n}}}{2} \tag{A8}$$

According to (1), we have:

$$\begin{cases} u_{\mathrm{v0}} - \dfrac{R_{\mathrm{arm}}}{3} i_{\mathrm{com}} - \dfrac{L_{\mathrm{arm}}}{3}\dfrac{\mathrm{d}i_{\mathrm{com}}}{\mathrm{d}t} + u_{\mathrm{Ceqcom}} = u_{\mathrm{com}} \\ u_{\mathrm{Ceqcom}} = \dfrac{1}{6}\sum\limits_{j=\mathrm{a,b,c}}\left(u_{\mathrm{p}j} - u_{\mathrm{n}j}\right) \end{cases} \tag{A9}$$

$$\begin{cases} -\dfrac{R_{\mathrm{arm}}}{3} i_{\mathrm{dif}} - \dfrac{L_{\mathrm{arm}}}{3}\dfrac{\mathrm{d}i_{\mathrm{dif}}}{\mathrm{d}t} + u_{\mathrm{Ceqdif}} = u_{\mathrm{dif}} \\ u_{\mathrm{Ceqdif}} = \dfrac{1}{6}\sum\limits_{j=\mathrm{a,b,c}}\left(u_{\mathrm{p}j} + u_{\mathrm{n}j}\right) \end{cases} \tag{A10}$$

APPENDIX B

$$\dot{\boldsymbol{i}}_{\mathrm{Ldc}} = \boldsymbol{L}_1\left[\boldsymbol{i}_{\mathrm{Ldc}} \quad \boldsymbol{i}_{\mathrm{LR}} \quad \boldsymbol{u}\right]^{\mathrm{T}} = \left[\boldsymbol{L}_{1\mathrm{a}} \quad \boldsymbol{L}_{1\mathrm{b}} \quad \boldsymbol{L}_{1\mathrm{c}}\right]\left[\boldsymbol{i}_{\mathrm{Ldc}} \quad \boldsymbol{i}_{\mathrm{LR}} \quad \boldsymbol{u}\right]^{\mathrm{T}} \tag{B1}$$

where

$$\boldsymbol{L}_{1\mathrm{a}} = \begin{bmatrix} \cdots & \cdots & \cdots & \cdots & \cdots \\ \cdots & -\dfrac{R_i}{L_{\mathrm{dc}} + mL_i} & -\dfrac{R_i}{L_{\mathrm{dc}} + mL_i} & -\dfrac{R_i}{L_{\mathrm{dc}} + mL_i} & \cdots \\ \cdots & -\dfrac{R_i}{L_{\mathrm{dc}} + mL_i} & -\dfrac{R_i}{L_{\mathrm{dc}} + mL_i} & -\dfrac{R_i}{L_{\mathrm{dc}} + mL_i} & \cdots \\ \cdots & -\dfrac{R_i}{L_{\mathrm{dc}} + mL_i} & -\dfrac{R_i}{L_{\mathrm{dc}} + mL_i} & -\dfrac{R_i}{L_{\mathrm{dc}} + mL_i} & \cdots \\ \cdots & \cdots & \cdots & \cdots & \cdots \end{bmatrix}$$

$$\boldsymbol{L}_{1\mathrm{b}} = \boldsymbol{0}$$

$$\boldsymbol{L}_{1\mathrm{c}} = \begin{bmatrix} \cdots & \cdots & \cdots & \cdots & \cdots \\ \cdots & -\dfrac{L_{\mathrm{dc}} + (m-1)L_i}{\left(L_{\mathrm{dc}} + mL_i\right)L_{\mathrm{dc}}} & \dfrac{L_i}{\left(L_{\mathrm{dc}} + mL_i\right)L_{\mathrm{dc}}} & 0 & \cdots \\ \cdots & \dfrac{L_i}{\left(L_{\mathrm{dc}} + mL_i\right)L_{\mathrm{dc}}} & -\dfrac{L_{\mathrm{dc}} + (m-1)L_i}{\left(L_{\mathrm{dc}} + mL_i\right)L_{\mathrm{dc}}} & 0 & \cdots \\ \cdots & \dfrac{L_i}{\left(L_{\mathrm{dc}} + mL_i\right)L_{\mathrm{dc}}} & \dfrac{L_i}{\left(L_{\mathrm{dc}} + mL_i\right)L_{\mathrm{dc}}} & 0 & \cdots \\ \cdots & \cdots & \cdots & \cdots & \cdots \end{bmatrix}$$

$$\boldsymbol{C}\dot{\boldsymbol{u}} = \boldsymbol{A}\left[\boldsymbol{i}_{\mathrm{Ldc}} \quad \boldsymbol{i}_{\mathrm{LR}} \quad \boldsymbol{i}_{\mathrm{s}}\right]^{\mathrm{T}} = \left[\boldsymbol{A}_{1\mathrm{a}} \quad \boldsymbol{A}_{1\mathrm{b}} \quad \boldsymbol{A}_{1\mathrm{c}}\right]\left[\boldsymbol{i}_{\mathrm{Ldc}} \quad \boldsymbol{i}_{\mathrm{LR}} \quad \boldsymbol{i}_{\mathrm{s}}\right]^{\mathrm{T}} \tag{B2}$$

where

$$\boldsymbol{C} = \left[\boldsymbol{C}_1 \quad \boldsymbol{C}_2\right]$$

$$\boldsymbol{C}_1 = \begin{bmatrix} \cdots & \cdots & \cdots & \cdots \\ \cdots & C_i & 0 & \cdots \\ \cdots & 0 & C_j & \cdots \\ \vdots & \vdots & \vdots & \vdots \\ \cdots & 0 & 0 & \cdots \\ \cdots & 0 & 0 & \cdots \\ \cdots & \cdots & \cdots & \cdots \end{bmatrix}$$

$$\boldsymbol{C}_2 = \begin{bmatrix} \cdots & \cdots & \cdots & \cdots \\ \cdots & 0 & 0 & \cdots \\ \cdots & 0 & 0 & \cdots \\ \vdots & \vdots & \vdots & \vdots \\ \cdots & \dfrac{C_{ij}}{2} + 2C_{\mathrm{M}ij} & 0 & \cdots \\ \cdots & 0 & \dfrac{C_{ij}}{2} + 2C_{\mathrm{M}ij} & \cdots \\ \cdots & \cdots & \cdots & \cdots \end{bmatrix}$$

$$\boldsymbol{A}_{1\mathrm{a}} = \begin{bmatrix} \cdots & \cdots & \cdots & \cdots & \cdots \\ \cdots & -1 & -1 & -1 & \cdots \\ \cdots & 0 & 0 & 0 & \cdots \\ \vdots & \vdots & \vdots & \vdots & \vdots \\ \cdots & 1 & 0 & 0 & \cdots \\ \cdots & 0 & 0 & 0 & \cdots \\ \cdots & \cdots & \cdots & \cdots & \cdots \end{bmatrix}$$

$$\boldsymbol{A}_{1\mathrm{b}} = \begin{bmatrix} \cdots & \cdots & \cdots \\ \cdots & 0 & \cdots \\ \cdots & 0 & \cdots \\ \vdots & \vdots & \vdots \\ \cdots & -1 & \cdots \\ \cdots & 1 & \cdots \\ \cdots & \cdots & \cdots \end{bmatrix}$$

$$\boldsymbol{A}_{1c}=\begin{bmatrix} \cdots & \cdots & \cdots & \cdots \\ \cdots & C_i & 0 & \cdots \\ \cdots & 0 & C_j & \cdots \\ \cdots & \cdots & \cdots & \cdots \\ \cdots & \cdots & \cdots & \cdots \\ \cdots & 0 & 0 & \cdots \\ \cdots & 0 & 0 & \cdots \\ \cdots & \cdots & \cdots & \cdots \end{bmatrix}$$

$$\dot{\boldsymbol{i}}_{LR}=\boldsymbol{L}_2\left[\boldsymbol{i}_{LR} \quad \boldsymbol{u}\right]^{T}=\left[\boldsymbol{L}_{2a} \quad \boldsymbol{L}_{2b}\right]\left[\boldsymbol{i}_{LR} \quad \boldsymbol{u}\right]^{T} \tag{B3}$$

where

$$\boldsymbol{L}_{2a}=\begin{bmatrix} \cdots & \cdots & \cdots & \cdots & \cdots \\ \cdots & -\dfrac{R_{ij}}{L_{ij}-M_{ij}} & 0 & 0 & \cdots \\ \cdots & 0 & -\dfrac{R_{ip}}{L_{ip}-M_{ip}} & 0 & \cdots \\ \cdots & 0 & 0 & -\dfrac{R_{iq}}{L_{iq}-M_{iq}} & \cdots \\ \cdots & \cdots & \cdots & \cdots & \cdots \end{bmatrix}$$

$$\boldsymbol{L}_{2b}=\begin{bmatrix} \cdots & \cdots & \cdots & \cdots & \cdots & \cdots & \cdots \\ \cdots & 0 & 0 & \cdots & \dfrac{1}{L_{ij}-M_{ij}} & -\dfrac{1}{L_{ij}-M_{ij}} & \cdots \\ \cdots & 0 & 0 & \cdots & 0 & 0 & \cdots \\ \cdots & 0 & 0 & \cdots & 0 & 0 & \cdots \\ \cdots & \cdots & \cdots & \cdots & \cdots & \cdots & \cdots \end{bmatrix}$$

REFERENCES

[1] W. Wang, M. Barnes, O. Marjanovic *et al.*, "Impact of DC breaker systems on multiterminal VSC-HVDC stability," *IEEE Transactions on Power Delivery*, vol. 31, no. 2, pp. 769-779, Apr. 2016.

[2] K. Sun, H. Xiao, J. Pan *et al*., "Cross-seam hybrid MTDC system for integration and delivery of large-scale renewable energy," *Journal of Modern Power Systems and Clean Energy*, vol. 9, no. 6, pp. 1352-1362, Nov. 2021.

[3] K. Sharifabadi, L. Harnefors, H. P. Nee *et al.*, "Introduction to modular multilevel converters," in *Design, Control and Application of Modular Multilevel Converters for HVDC Transmission Systems*. Chichester: Wiley, 2016, pp. 7-17.

[4] M. Saltzer, "Surge and extended overvoltage testing of HVDC cable systems," in *Proceedings of International Conference on Insulated Power Cables*, Dunkerque, France, Nov. 2017, pp. 1-7.

[5] R. Hong, "Architecture of Nan'ao multi-terminal VSC-HVDC system and its multi-functional control," *CSEE Journal of Power and Energy Systems*, vol. 1, no. 1, pp. 9-18, Mar. 2015.

[6] T. Westerweller, A. Orini, D. Parquet *et al*., "Trans Bay cable–world's first HVDC system using multilevel voltage-sourced converter," in *Proceedings of CIGRE*, France, Paris, Jan. 2010, pp. 1-10.

[7] T. M. L. Assis, S. Kuenzel, and B. C. Pal, "Impact of multi-terminal HVDC grids on enhancing dynamic power transfer capability," *IEEE Transactions on Power Systems*, vol. 32, no. 4, pp. 2652-2662, Jul. 2017.

[8] K. Koreman, Y. Fu, F. Hassan *et al*., "Protection and local control of HVDC grids," in *Proceedings of CIGRE*, France, Paris, Aug. 2018, pp. 1-12.

[9] R. Li, L. Xu, D. Holliday *et al*., "Continuous operation of radial multiterminal HVDC systems under DC fault," *IEEE Transactions on Power Delivery*, vol. 31, no. 1, pp. 351-361, Feb. 2016.

[10] N. A. Belda, C. Plet, and R. P. Smeets, "Analysis of faults in multi-terminal HVDC grid for definition of test requirements of HVDC circuit breakers," *IEEE Transactions on Power Delivery*, vol. 33, no. 1, pp. 403-411, Feb. 2017.

[11] O. Cwikowski, H. Wickramasinghe, G. Konstantinou *et al*., "Modular multilevel converter DC fault protection," *IEEE Transactions on Power Delivery*, vol. 33, no. 1, pp. 291-300, Feb. 2017.

[12] F. B. Ajaei and R. Iravani, "Cable surge arrester operation due to transient overvoltage under DC-side faults in the MMC-HVDC link," *IEEE Transactions on Power Delivery*, vol. 31, no. 3, pp. 1213-1222, Jun. 2016.

[13] S. Dennetière, H. Saad, A. Naud *et al*., "Transients on DC cables connected to VSC converters," in *Proceedings of International Conference on Insulated Power Cables*, Versailles, France, Jun. 2015, pp. 1-6.

[14] M. Goertz, "Overvoltage characteristics in symmetrical monopole HB MMC-HVDC configuration comprising long cable systems," in *Proceedings of International Conference on Power System Transients*, Perpignan, France, Jun. 2019, pp. 1-6.

[15] S. Mukherjee, M. Saltzer, Y. J. Häfner *et al*., "Cable overvoltage for MMC based VSC HVDC systems: interactions with converters," in *Proceedings of International Colloquium on High Voltage Insulated Cables*, New Delhi, India, Oct. 2017, pp. 1-7.

[16] H. Wang, J. Cao, Z. He *et al*., "Research on overvoltage for XLPE cable in a modular multilevel converter HVDC transmission system," *IEEE Transactions on Power Delivery*, vol. 31, no. 2, pp. 683-692, Apr. 2016.

[17] H. Saad, P. Rault, and S. Dennetière, "Study on transient overvoltage in the converter station of HVDC-MMC links," in *Proceedings of International Conference on Power System Transients*, Seoul, South Korea, Jun. 2017, pp. 1-7.

[18] J. Yu, Z. Zhang, Z. Xu *et al*., "An equivalent calculation method for pole-to-ground fault transient characteristics of symmetrical monopolar MMC based DC grid," *IEEE Access*, vol. 8, pp. 123952-123965, Jun. 2020.

[19] E. D. Kimbark, "Transient overvoltage caused by monopolar ground fault on bipolar DC line: theory and simulation," *IEEE Transactions on Power Apparatus Systems*, vol. PAS-89, no. 4, pp. 584-592, Apr. 1970.

[20] Z. He, J. Hu, L. Lin *et al*., "Pole-to-ground fault analysis for HVDC grid based on common- and differential-mode transformation," *Journal of Modern Power Systems and Clean Energy*, vol. 8, no. 3, pp. 521-530, May 2020.

[21] S. Xue, J. Lian, J. Qi *et al*., "Pole-to-ground fault analysis and fast protection scheme for HVDC based on overhead transmission lines," *Energies*, vol. 10, no. 7, pp. 1059-1076, Jul. 2017.

[22] R. Li, J. E. Fletcher, L. Xu *et al*., "Enhanced flat-topped modulation for MMC control in HVDC transmission systems," *IEEE Transactions on Power Delivery*, vol. 32, no. 1, pp. 152-161, Feb. 2017.

[23] H. Saad, S. Dennetiere and J. Mahseredjian *et al*., "Modular multilevel converter models for electromagnetic transients," *IEEE Transactions on Power Delivery*, vol. 29, no. 3, pp. 1481-1489, Jun. 2014.

[24] Q. Tu and Z. Xu, "Impact of sampling frequency on harmonic distortion for modular multilevel converter," *IEEE Transactions on Power Delivery*, vol. 26, no. 1, pp. 298-306, Jan. 2011.

[25] Z. Xu, "Working principle of MMC basic unit," in *Flexible DC Transmission System*, 2nd ed. Beijing: China Machine Press, 2016, pp. 19-23.

[26] L. Xiao, Z. Xu, T. An *et al*., "Improved analytical model for the study of steady state performance of droop-controlled VSC-MTDC systems," *IEEE Transactions on Power Systems*, vol. 32, no. 3, pp. 2083-2093, May 2017.

[27] S. Gao, H. Ye, and Y. Liu, "Accurate and efficient estimation of short-circuit current for MTDC grids considering MMC control," *IEEE Transactions on Power Delivery*, vol. 35, no. 3, pp. 1541-1552, Jun. 2020.

[28] N. Yousefpoor, A. Narwal, and S. Bhattacharya, "Control of DC-fault resilient voltage source converter-based HVDC transmission system under dc fault operating condition," *IEEE Transactions on Industrial Electronics*, vol. 62, no. 6, pp. 3683-3690, Jun. 2015.

[29] J. Yu, Z. Zhang, and Z. Xu, "A local protection and local action strategy of DC grid fault protection," *Energies*, vol. 13, no. 18, pp. 4795-4808, Sept. 2020.

[30] S. Yan, Z. He, J. Yang *et al*., "Optimized protection strategies for HVDC grid with fault-blocking modular multilevel converters for overhead line applications," *Journal of Modern Power Systems and Clean Energy*, vol. 8, no. 6, pp. 1168-1177, Nov. 2020.

Jingqiu Yu received the B.S. degree in electrical engineering from Wuhan University, Wuhan, China, in 2018. Now, he is pursuing the Ph.D. degree in electrical engineering at Zhejiang University, Hangzhou, China. His research interests include overvoltage and insulation coordination of DC systems.

Zheren Zhang received the B.S. and Ph.D degrees in electrical engineering from Zhejiang University, Hangzhou, China, in 2011 and 2016, respectively. He is now with the Department of Electrical Engineering, Zhejiang University. His research interests include high-voltage direct current (HVDC), flexible AC transmission systems (FACTS), and grid integration of renewable energy.

Zheng Xu received the B.S., M.S., and Ph.D. degrees in electrical engineering from Zhejiang University, Hangzhou, China, in 1983, 1986, and 1993, respectively. He has been with the Department of Electrical Engineering, Zhejiang University, since 1986, and has been a Professor there since 1998. He is a Fellow of IEEE for his contributions to control and modeling of modular multilevel converter (MMC) based high-voltage direct current (HVDC) transmission systems. His research interests include HVDC, flexible AC transmission systems (FACTS), and grid integration of renewable energy.